Analytical treatment of ultrafast laser-induced spin-flipping Λ processes on magnetic nanostructures

Georgios Lefkidis* and Wolfgang Hübner

Department of Physics and Research Center OPTIMAS, University of Kaiserslautern, PO Box 3049, 67653 Kaiserslautern, Germany

(Received 13 August 2012; revised manuscript received 21 November 2012; published 3 January 2013)

In this paper, we analytically treat ultrafast, laser-induced, spin-flipping processes based on Λ model systems with triplet ground state. After obtaining the wave functions, we give analytical solutions for the induced material polarization in the time domain. Compact summation formulas for the time-dependent (windowed) induced polarization of the material in the frequency domain, as well as its helicity (fourth Stokes parameter), are given. These solutions compare excellently with numerical results obtained for realistic systems (i.e., systems that can or have been synthesized and were treated with high-level quantum chemical methods including electron correlations and relativistic effects). We thus analytically show that laser-induced spin flip is possible and can be detected from the helicity of the emitted light during the process. Additionally, we analyze the effects of a finite temperature and the time window of a measuring apparatus on the signal detected. These are very crucial steps not only for verifying the validity of previous numerical results, but also for the deeper understanding of the physical mechanisms involved.

DOI: 10.1103/PhysRevB.87.014404 PACS number(s): 78.20.Bh, 42.50.−p, 75.78.Jp

I. INTRODUCTION

Ever since the discovery of laser-induced, ultrafast demagnetization in magnetically ordered materials,[1] optical manipulation of the spin degree of freedom on the subpicosecond scale has been the object of intense theoretical and experimental research since the relevant electronics applications may satisfy the growing industrial interest for speed upgrade and size downscale of computer elements.[1–6] Although there is an ongoing discussion about the exact nature of all participating mechanisms at different time scales, there seems to be a consensus that (at least to some extent) light can serve as an angular momentum reservoir.[5–7] In a previous work, we presented numerical results which show that during a spin-flipping Λ process, the material absorbs and emits the correct light helicity provided that it is present in the environment (our calculations were performed within the semiclassical approximation, therefore the presence of light is necessary for emission as well).[8] In this paper, we delve deeper into the nature of the mechanisms involved and present an analytic treatment of this scenario on a model Λ system, which is in perfect accord with the numerical results obtained for the highly complicated case studied in Ref. 8. Furthermore, this analytical model is capable of describing laser-induced spin-flipping processes on magnetic materials with triplet ground state and strongly localized spin density. Such materials can comprise, among others, linear or branched metallic chains deposited on inert surfaces,[9–11] metallic clusters in the gas phase (with or without chromophores such as CO as experimental magnetic-state markers),[12] and ligand-stabilized complexes in solution.[13,14] For the time evolution of the system, we use a wave function rather than a density-matrix approach exploited by other authors (see Refs. 15–17 and references therein). This is mainly in order to follow the same formalism we use for our numerical results applied to small, real-space objects (more convenient and numerically more stable).

Although analytical solutions to the time-dependent Schrödinger equation describing a driven system are extremely rare,[18] some three-level systems have already been extensively investigated in the past.[19] However, almost all of them have concentrated on the effect of the laser pulse on the system with respect to its magnetization. Chen *et al.* have investigated arbitrary rotations of the spin of a single electron in a quantum dot via Raman transitions in the adiabatic limit,[20] while Wu *et al.* have looked upon the selective excitation from the spin ground states to the trion state through phase-sensitive control. The mechanism they use is an external magnetic field in the Voigt geometry, in which the trion states remain unaffected (pertinent to semiconductors).[21] Bao *et al.* have studied the nonlocal behavior of measurements performed on many electrons and presented a microscopic theory of impulsive stimulated Raman scattering and multispin entanglement.[22] At the same time, purely theoretical studies have dealt with additional relativistic corrections due to the field of the pulse[23] and susceptibility during laser-induced magnetism control.[24] Here, we go one step further and we look into the role of the polarization of the light in the angular momentum conservation of the spin-flipping process, which is identified in the induced polarization of the material. This way, we go beyond classical models based on the the Landau-Lifshitz-Gilbert types (and derivatives) of equations of motion.[25]

The paper is organized as follows: first the model and the derivation of the transition matrix elements are presented both for the degenerate and the quasidegenerate initial and final states (Sec. II), followed by the analysis for finite temperatures (Sec. III). Finally, some general conclusions are drawn (Sec. IV).

II. THE Λ PROCESS

For our model Hamiltonian, we assume a three-level system ($|a\rangle$, $|b\rangle$, and $|c\rangle$ are the initial, final, and intermediate states, respectively). The main idea of a Λ process is that the initial and the final states are (quasi)degenerate, while the intermediate state is energetically far away and optically addressable (with electric-dipole transitions), so instead of a slow direct transition $|a\rangle \rightarrow |b\rangle$, we first excite to the intermediate state and then deexcite to the final state $|a\rangle \rightarrow |c\rangle \rightarrow |b\rangle$ which can

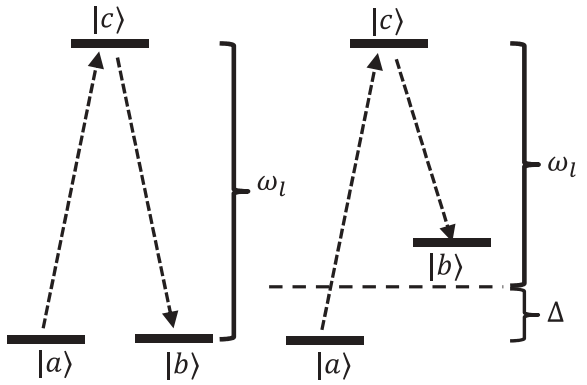

FIG. 1. Λ systems. Left panel: degenerate case; right panel: symmetric nondegenerate case.

be a far faster process (Fig. 1). For our scenarios we use a single laser pulse to drive both transitions. Depending on the particular properties of the initial and the final states, one can derive different scenarios which can lead to optical, coherent manipulation of the magnetization of the system on the subpicosecond scale. So (a) if the two states exhibit parallel magnetization with different magnitude of the magnetization vectors, we have (partial) demagnetization, (b) if the magnetization vectors are antiparallel and the spin density is localized on the same atom (e.g., spin-up and -down terms of the same singlet or triplet state) we have spin flip, and (c) if the two magnetization vectors are parallel to each other but the spin density is localized on different atoms, we have spin transfer. Conceptually one can think of a fourth case as well, which is a combination of cases (b) and (c), i.e., simultaneous spin flip and spin transfer, a scenario which, however, we have not been able to achieve on any realistic system thus far. In the case of spin-flip processes [(b) or (d)], the intermediate state needs to be addressable from states with different spin orientation and thus has to be spin mixed. Here, the spin mixing results from spin-orbit coupling (SOC) which accordingly changes the optical selection rules.[8,26]

A. Degenerate case

We build our Λ system (Fig. 1, left panel) choosing the states as follows. The initial ground state and the final ground state are the spin-down and -up triplets of an S state, respectively. So, we have $|a\rangle = |0,0\rangle \otimes |\downarrow\downarrow\rangle$ and $|b\rangle = |0,0\rangle \otimes |\uparrow\uparrow\rangle$. The intermediate state is the $|j = 1, m_j = 0\rangle$ term ($^3P_1$) resulting from the consideration of SOC in an excited triplet P state (the use of SOC splits the triplet ^3P to a quintet $^3P_2$, a triplet $^3P_1$, and a singlet $^3P_0$ in spectroscopic notation $^{2s+1}L_j$; j refers to the total angular momentum when spin and orbital angular momentum are coupled). Using Clebsch-Gordan coefficients (or diagonalizing the respective SOC Hamiltonian), we find that

$$|c\rangle = |j = 1, m_j = 0\rangle = \frac{1}{\sqrt{2}}\left(|1,1\rangle \otimes |\downarrow\downarrow\rangle - |1,-1\rangle \otimes |\uparrow\uparrow\rangle\right),$$

where $|1,\pm 1\rangle = p_\pm = \frac{1}{\sqrt{2}}\left(p_x \pm i p_y\right)$ (note that the two numbers in the ket refer to the eigenvalues l and l_z of the orbital angular momentum, unless explicitly specified otherwise). We can then calculate the transition matrix elements

$$\begin{aligned}
\langle a|\hat{x}|c\rangle &= \frac{1}{\sqrt{2}}\langle 0,0|\hat{x}|1,1\rangle \\
&= \frac{1}{2}\left(\langle s|\hat{x}|p_x\rangle + i\langle s|\hat{x}|p_y\rangle\right) = 2\mu, \\
\langle b|\hat{x}|c\rangle &= -\frac{1}{\sqrt{2}}\langle 0,0|\hat{x}|1,-1\rangle \\
&= -\frac{1}{2}\left(\langle s|\hat{x}|p_x\rangle - i\langle s|\hat{x}|p_y\rangle\right) = -2\mu, \\
\langle a|\hat{y}|c\rangle &= \frac{1}{\sqrt{2}}\langle 0,0|\hat{y}|1,1\rangle \\
&= \frac{1}{2}\left(\langle s|\hat{y}|p_x\rangle + i\langle s|\hat{y}|p_y\rangle\right) = i2\mu, \\
\langle b|\hat{y}|c\rangle &= -\frac{1}{\sqrt{2}}\langle 0,0|\hat{y}|1,-1\rangle \\
&= -\frac{1}{2}\left(\langle s|\hat{y}|p_x\rangle - i\langle s|\hat{y}|p_y\rangle\right) = i2\mu
\end{aligned}$$

with $\langle s|\hat{x}|p_x\rangle = \langle s|\hat{y}|p_y\rangle = 4\mu$ [we set the integral equal to 4μ in order to simplify the equations of motion of the system, Eqs. (1)]. The integrals $\langle s|\hat{x}|p_y\rangle = \int f_s(r) y f_{p_x}(r)\, dV$ and $\langle s|\hat{x}|p_y\rangle = \int f_s(r) x f_{p_y}(r)\, dV$ vanish [$f_s(r)$, $f_{p_x}(r)$, and $f_{p_y}(r)$ are the radial parts of the wave functions of the states $|s\rangle$, $|p_x\rangle$, and $|p_y\rangle$, respectively].[27] In fact, for this system one can always make the perturbation element $\hat{H}'_{ij}(t) = \mathbf{E}(t)\cdot\langle i|\hat{\mathbf{r}}|j\rangle$ real by a proper choice of the time origin. We start our investigation with the simplest case, when (i) the initial and the final states are degenerate ($E_a = E_b = 0$), and (ii) the transition matrix elements between those states and the intermediate state $|c\rangle$ have equal magnitudes ($|\mu_{ac}| = |\mu_{cb}| = \mu$). The system is irradiated with a linearly polarized laser pulse $\mathbf{E} = (E_x, 0, 0)$. (Due to the generality of the formulas used, we do not discuss units in the manuscript and for simplicity we also set $\hbar = 1$. The only assumption is that the value of μ is small enough to make the time-dependent perturbation theory applicable.)

Adopting the interaction picture, we get a system of coupled ordinary differential equations. In the simplest case, the laser pulse is resonant to the excitation energy $\omega_l = E_c - E_a = E_c - E_b$. This can be achieved, if one eliminates any phase difference, by proper tilting of the laser pulse (numerical results indicate that for this energy difference the phase is not important). The initial conditions are $a(0) = 1$ and $b(0) = c(0) = 0$. The system has constant coefficients and can thus be solved with the matrix method. Then, the phase factors are attached [the differential equation system is in the interaction picture and within the rotating-wave approximation (RWA)]:

$$\dot{a}(t) = -i\mu\, c(t), \quad \dot{b}(t) = i\mu\, c(t), \quad \dot{c}(t) = -i\mu\,[a(t) - b(t)] \tag{1}$$

with the well-known solution[28–30]

$$a(t) = \frac{1}{2}[1 + \cos(\sqrt{2}\mu t)], \quad b(t) = \frac{1}{2}[1 - \cos(\sqrt{2}\mu t)], \quad c(t) = -\frac{i}{\sqrt{2}}\sin(\sqrt{2}\mu t). \tag{2}$$

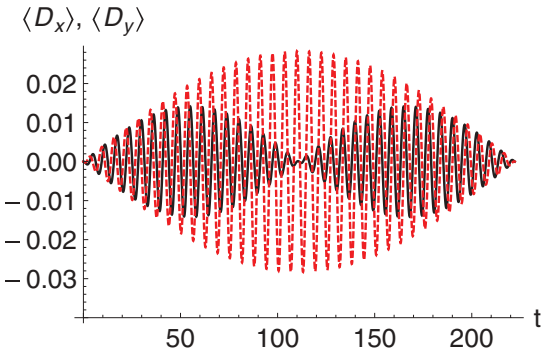

FIG. 2. (Color online) Time evolution of the induced polarization in the material for the symmetric system ($\omega_l = 1$ and $\mu = 0.01$). The black solid line is the $\langle D_x(t)\rangle$ and the red dashed line the $\langle D_y(t)\rangle$ component. Note their relative phase difference at early and late times connected to the absorption and emission phases of the Λ process, respectively (relate to Fig. 1, left panel). This clearly indicates different helicities of absorbed and emitted light, a fact which, in turn, is in line with the total angular momentum conservation of the system and the light (Ref. 8).

The population of the final state is $P_b(t) = \frac{1}{4}[1 - \cos(\sqrt{2}\mu t)]^2$ and gets maximized at time $t_{\max} = \frac{k\pi}{\sqrt{2}\mu}$ where k is an odd integer. Note that since we are working in the interaction picture, a phase factor $e^{-iE_c t}$ must be attached to the wave function of the excited state $|c\rangle$ (if we define $E_a = E_b = 0$, this is not necessary for $|a\rangle$ and $|b\rangle$ since $e^{-iE_a t} = e^{-iE_b t} = e^0 = 1$). So, the total wave function of the system becomes $|\Psi(t)\rangle = a(t)|a\rangle + b(t)|b\rangle + c(t)e^{-iE_c t}|c\rangle$. We calculate the density matrix of the system $\rho(t) = |\Psi(t)\rangle\langle\Psi(t)|$ and with the use of the electric-dipole transition matrices

$$\mathbf{D}_x = 2\mu\begin{pmatrix} 0 & 0 & 1 \\ 0 & 0 & -1 \\ 1 & -1 & 0 \end{pmatrix}, \quad \mathbf{D}_y = 2\mu\begin{pmatrix} 0 & 0 & i \\ 0 & 0 & i \\ -i & -i & 0 \end{pmatrix},$$

we get for the expectation values of the components of the induced polarization[31]

$$\begin{aligned} \langle D_x(t)\rangle &= \mathrm{Tr}[\rho(t)\mathbf{D}_x] = -\sqrt{2}\mu\sin(2\sqrt{2}\mu t)\sin(\omega_l t), \\ \langle D_y(t)\rangle &= \mathrm{Tr}[\rho(t)\mathbf{D}_y] = -2\sqrt{2}\mu\sin(\sqrt{2}\mu t)\cos(\omega_l t), \end{aligned} \tag{3}$$

where ω_l is the resonant laser frequency. Since we are interested in the time-dependent polarizations during the pulse (when the intermediate states also get populated), we need the full 3×3 density matrix; this would not be necessary if we investigated the system only *after* the pulse.[21] The resulting interferences are of quantum nature since only one laser pulse is involved (as opposed to Blanchet *et al.* who use two identical laser pulses).[32] As one can clearly see in Fig. 2, the phase difference between the x and the y components alternates in sign, meaning that during half of the period (which corresponds to the absorption phase) the induced polarization has one helicity (σ_+), while during the second half of the period (the emission phase of the Λ process) it has the opposite helicity (σ_-). This finding can be quantified by calculating the time-resolved Stokes vector $\mathbf{S}$ for the induced polarization $\mathbf{D}(t)$. To this end, we Fourier transform Eqs. (3) using a Gaussian distribution with standard deviation σ:

$$G(\sigma, t - t') = \frac{1}{\sqrt{2\pi\sigma^2}} e^{-\frac{(t-t')^2}{2\sigma^2}} \tag{4}$$

as the normalized time-dependent window function. For the actual calculations, it is important to choose a σ that extends over several periods of the laser frequency, otherwise the frequencies get erroneously blue-shifted. After integration and some lengthy but rather straightforward algebraic manipulations, we arrive at two compact summation formulas

$$\begin{aligned} \tilde{D}_x(\omega,t) &= \int_{-\infty}^{\infty} \langle D_x(t')\rangle G(\sigma, t - t') e^{i\omega t'}\, dt' \\ &= \frac{\mu}{2\sqrt{2}} \sum_{k=1}^{4} (-1)^k e^{iA_k t - \frac{1}{2}\sigma^2 A_k^2}, \end{aligned} \tag{5}$$

$$\begin{aligned} \tilde{D}_y(\omega,t) &= \int_{-\infty}^{\infty} \langle D_y(t')\rangle G(\sigma, t - t') e^{i\omega t'}\, dt' \\ &= \frac{i\mu}{2\sqrt{2}} \sum_{k=1}^{4} (-1)^k e^{iB_k t - \frac{1}{2}\sigma^2 B_k^2}, \end{aligned} \tag{6}$$

where the real constants A_k and B_k are given by

$$\begin{aligned} A_1 &= \omega + \omega_l - 2\sqrt{2}\mu, \quad A_2 = \omega + \omega_l + 2\sqrt{2}\mu, \\ A_3 &= \omega - \omega_l + 2\sqrt{2}\mu, \quad A_4 = \omega - \omega_l - 2\sqrt{2}\mu, \\ B_1 &= \omega - \omega_l - \sqrt{2}\mu, \quad B_2 = \omega + \omega_l + \sqrt{2}\mu, \\ B_3 &= \omega + \omega_l - \sqrt{2}\mu, \quad B_4 = \omega - \omega_l + \sqrt{2}\mu \end{aligned} \tag{7}$$

[the order of A_k and B_k with respect to the signs is intentionally not the same, so that the factors $(-1)^k$ in the sums of Eqs. (5) and (6) give the correct signs]. Note that Eqs. (5) and (6) approach the exact (nonwindowed) Fourier transform of $\langle D_x(t)\rangle$ and $\langle D_y(t)\rangle$ for $\sigma \to \infty$, as expected. Since $\mu \ll \omega$, when investigating the behavior around the light frequency, one could in principle even omit the terms involving $\omega + \omega_l$, something that would be in line with the RWA used. We see that the frequencies of $\tilde{D}_x(\omega,t)$ and $\tilde{D}_y(\omega,t)$ have slightly different time-dependent phase factors ($e^{iA_k t}$ and $e^{iB_k t}$, respectively), which lead to alternating time ordering of their respective maxima and minima (Fig. 2). The helicity of the circular polarization is given by the sign of the fourth component of the Stokes vector $\mathbf{S}(I, Q, U, V)$:

$$\begin{aligned} V(\omega,t) &= 2\,\mathrm{Im}[\tilde{D}_y^*(\omega,t)\tilde{D}_x(\omega,t)] \\ &= -\frac{\mu^2}{2} \sum_{\substack{j=1 \\ k=1}}^{4} \{(-1)^{j+k} \cos[(A_j - B_k)t] e^{-\frac{1}{2}\sigma^2(A_j^2 + B_k^2)}\}. \end{aligned} \tag{8}$$

Figure 3 shows the induced polarization in the system, i.e., the fourth component of the Stokes vector $V(\omega,t)$ during a full period. Note here that the choice of the width of the window function through σ influences the shape of the peaks: a wide window gives better frequency but worse time resolution, while a narrow window gives an enhanced time and reduced frequency resolution (narrow-band and wide-band transforms). The peaks are not symmetrically located around the resonant laser frequency (taken to be 1 in Fig. 3) but

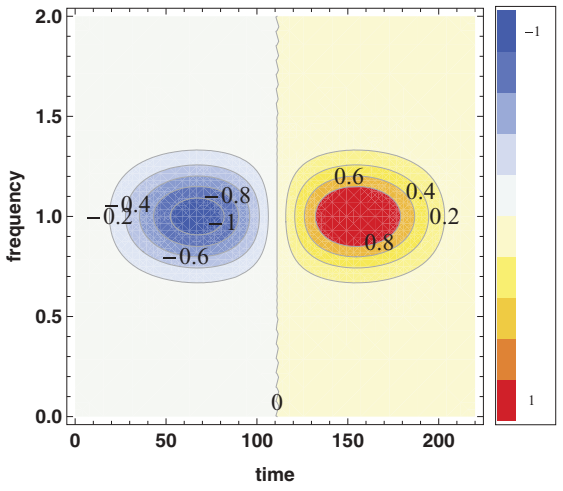

FIG. 3. (Color online) Fourth component $V(\omega,t)$ of the Stokes vector indicating the helicity of the induced polarization in the system ($\omega_l = 1$, $\sigma = 4$, $\mu = 0.01$). The different helicities between absorption (σ_+) and emission (σ_-) phases are evident (Ref. 8). $V(\omega,t)$ is magnified 30 000 times.

slightly extend to higher frequencies (not visible in Fig. 3). The reason is that the occupations of the levels change with time (if the transition matrix elements become infinitesimal, then the center of the peak is at the same frequency as the laser pulse). These analytical results are completely consistent and further corroborate the numerical results on a realistic system published previously.[8]

It is clear that the width of the weighting window, given by the experimental setup of the measurement apparatus and mathematically expressed by σ, influences the result of the measurement (Fig. 4). If σ is too large with respect to the population transfer time $t_{\max}$, then the measured light becomes falsely linearly polarized simply because the experiment averages out the absorption and the emission phase. If it is too small, then it does not correctly capture the frequency.

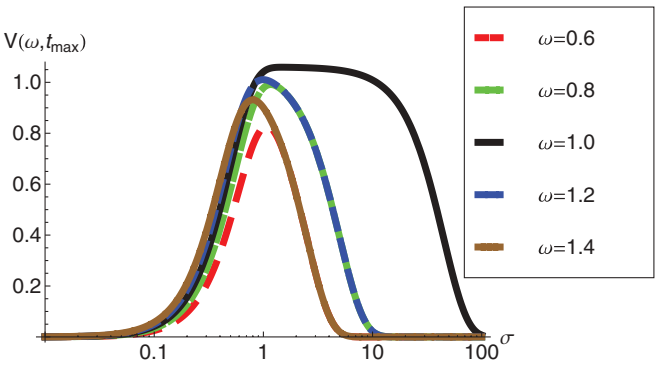

FIG. 4. (Color online) Maximal magnitude of the fourth component of the Stokes vector $V_{\max} = V(\omega,t_{\max})$ vs σ (in logarithmic scale). $\mu = 0.01$ and $\omega_l = 1$. The black solid line is for the resonant frequency $\omega = \omega_l$, the red dashed lines are for smaller and the green dotted lines for larger frequencies. Changing the magnitude of the transition matrix elements μ does not change the shape or magnitude of $V_{\max}$ and only moves the lines to smaller or larger σ values (for larger and smaller μ values, respectively). $V_{\max}$ is magnified 30 000 times.

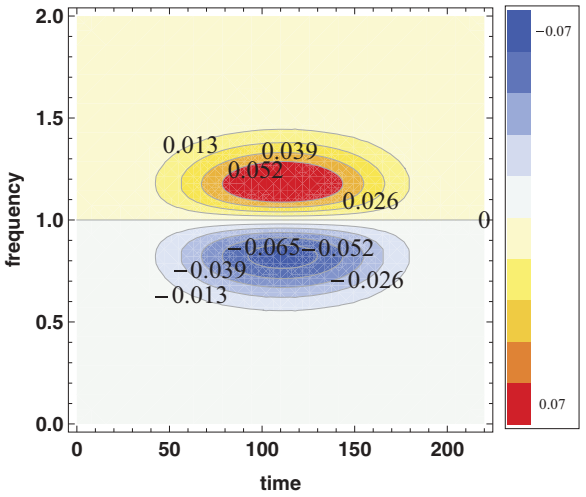

FIG. 5. (Color online) Third component $U(\omega,t)$ of the Stokes vector indicating the linear induced polarization in the system along the quadrant bisectors ($\omega_l = 1$, $\sigma = 4$, $\mu = 0.01$). $U(\omega,t)$ is magnified 30 000 times.

One can also calculate the other Stokes parameters, e.g., the third parameter $U(\omega,t)$ which gives the linear polarization along the $x - y$ diagonals (Fig. 5):

$$U(\omega,t) = 2\,\mathrm{Re}[\tilde{D}_y^*(\omega,t)\tilde{D}_x(\omega,t)] = -\frac{\mu^2}{2}\sum_{\substack{j=1\\k=1}}^{4}\left\{(-1)^{j+k}\sin[(A_j - B_k)t]e^{-\frac{1}{2}\sigma^2(A_j^2+B_k^2)}\right\}. \tag{9}$$

We see a that there is a splitting of the linear polarization in this direction: For slightly higher than resonant frequencies ($\omega > \omega_0$), the polarization plane is in the I and III quadrants, while for slightly lower energies ($\omega < \omega_0$), the plane is in the II and IV quadrants (parallel to the z axis). For $\omega = \omega_0$, the two cancel out at all times.

B. Symmetric nondegenerate case

If the initial and final states are nondegenerate and the pulse is set to the mean value of the two resonances $\omega_l = E_c - \frac{1}{2}(E_a + E_b)$, in which case we can define $E_c - E_a - \omega_l = \Delta$ and $E_c - E_b - \omega_l = -\Delta$, the system can still be analytically solved (Fig. 1, right panel). The system of the differential equations within the interaction picture and using the RWA becomes

$$\dot{a}(t) = -i\mu c(t)e^{-i\Delta t}, \quad \dot{b}(t) = i\mu c(t)e^{i\Delta t}, \quad \dot{c}(t) = -i\mu \underbrace{[a(t)e^{i\Delta t} - b(t)e^{-i\Delta t}]}_{=f(t)} \tag{10}$$

or

$$\dot{a}(t)e^{i\Delta t} = -i\mu c(t), \quad \dot{b}(t)e^{-i\Delta t} = i\mu c(t), \quad \dot{c}(t) = -i\mu f(t) \tag{11}$$

with the same initial conditions as in the degenerate case. By differentiating the newly defined function $f(t)$, one easily finds that $\ddot{f}(t) + \Omega^2 f(t) = 0$ with $\Omega = \sqrt{2\mu^2 + \Delta^2}$ and initial conditions $f(0) = a(0)e^0 - b(0)e^0 = 1$ and $\dot{f}(0) =$

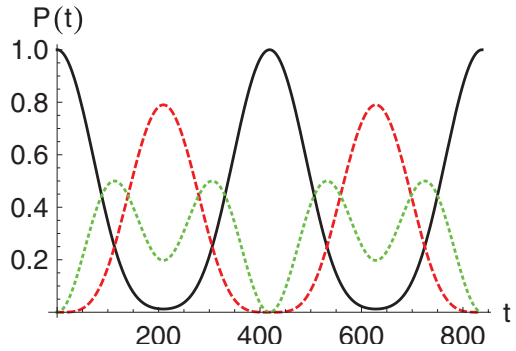

FIG. 6. (Color online) Time-dependent populations for symmetric detuning $\Delta = 0.005$, $\omega_l = 1$ and transition matrix elements $\mu_{ac} = \mu_{cb} = 0.01$. The black solid line is the population of the initial state $|a\rangle$, the red dashed line the population of the final state $|b\rangle$, and the dotted green line the population of the intermediate state $|c\rangle$.

$-i2\mu c(0) + i\Delta[a(0)e^0 + b(0)e^0] = i\Delta$. From its solution and Eqs. (11), we can find $c(t)$:

$$f(t) = \cos(\Omega t) + \frac{i\Delta}{\Omega}\sin(\Omega t) \Rightarrow$$
$$c(t) = \frac{\mu\Delta}{\Omega^2}[1 - \cos(\Omega t)] - \frac{i\mu}{\Omega}\sin(\Omega t).$$

Now we can find $a(t)$ and $b(t)$ by integrating and taking into account the boundary conditions. The resulting ground-state wave-function coefficients become

$$a(t) = \left[\Omega\cos\left(\frac{\Omega t}{2}\right) + i\Delta\sin\left(\frac{\Omega t}{2}\right)\right]^2 \frac{e^{-i\Delta t}}{\Omega^2},$$
$$b(t) = 2\sin^2\left(\frac{\Omega t}{2}\right)\frac{\mu^2 e^{i\Delta t}}{\Omega^2}. \tag{12}$$

Figure 6 shows the resulting population for a sinusoidal laser pulse. Note that the magnitude of the transition matrix elements affects only the period, and not the maximum transfer achieved. This means that a nonresonant system ($\Delta \neq 0$) can never exhibit a full population transfer (see Fig. 7). It is important however, that the value of μ does not become too strong with respect to the energy separation of the states (ω), otherwise the time-dependent perturbation theory applied [Eq. (10)] is no longer valid.

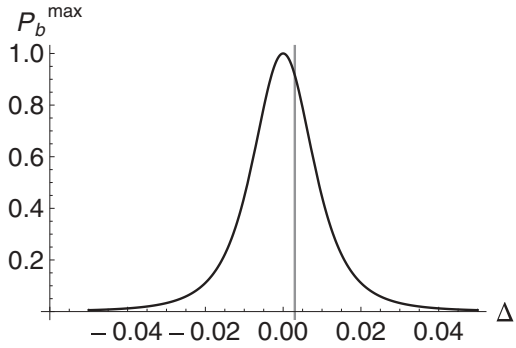

FIG. 7. Maximum population transfer $P_b^{\max}$ in the case of symmetric detuning Δ and transition matrix elements $\mu_{ac} = \mu_{cb} = 0.01$. For $\Delta \to 0$, we get the degenerate case and a 100% population transfer. The horizontal line at $\Delta = 0.003$ corresponds to Fig. 8.

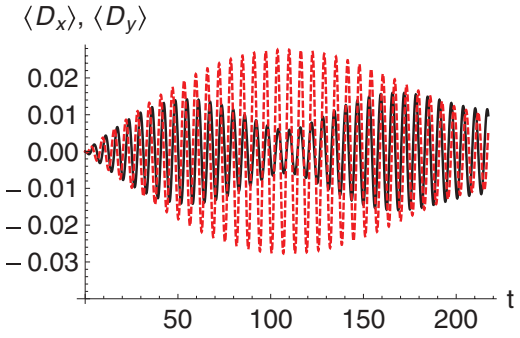

FIG. 8. (Color online) Time evolution of the induced polarization in the material for the quasidegenerate system ($\Delta = 0.003$, $\omega_l = 1$, and $\mu = 0.01$). The black solid line is the $\langle D_x(t)\rangle$ and the red dashed line the $\langle D_y(t)\rangle$ component. Note again their relative phase difference at early (absorption) and late (emission) times (see also Fig. 1, right panel). Unlike the degenerate case (Fig. 2), the plot is no longer symmetric.

The population of the final (target) state is

$$P_b(t) = b^*(t)b(t) = 4\left[\frac{\mu}{\Omega}\sin\left(\frac{\Omega t}{2}\right)\right]^4 \tag{13}$$

and first attains its maximum value $P_b^{\max} = \frac{4\mu^4}{\Omega^4}$ at time $t_{\max} = \frac{\pi}{\Omega}$ (see Figs. 6 and 7).

We can again calculate the expectation values of the time-dependent, induced material polarization:

$$\langle D_x(t)\rangle = -\frac{4\mu^2}{\Omega^3}\left\{2\Delta\Omega\cos(\omega_l t)\sin^2\left(\frac{\Omega t}{2}\right) + [\Delta^2 + 2\mu^2\cos(\Omega t)]\sin(\Omega t)\sin(\omega_l t)\right\}, \tag{14}$$

$$\langle D_y(t)\rangle = \frac{4\mu^2}{\Omega^4}\left\{2\Delta[\Delta^2 + 2\mu^2\cos(\Omega t)]\sin^2\left(\frac{\Omega t}{2}\right)\sin(\omega_l t) - \Omega^3\cos(\omega_l t)\sin(\Omega t)\right\} \tag{15}$$

[note that for $\Delta = 0$, these equations reduce to Eqs. (3)]. The behavior of the helicity of the induced material polarization is again similar to the degenerate case (Fig. 8).

Fourier transforming with a Gaussian window results in similar, although more complicated, summation formulas. If we keep only the terms with amplitudes of zeroth order with respect to Δ, we get (for the full formulas, see the Appendix)

$$\tilde{D}_x(\omega,t) = \frac{\mu^2}{\Omega^3}\sum_{k=1}^{4}(-1)^k e^{iA_k t - \frac{1}{2}\sigma^2 A_k^2},$$
$$\tilde{D}_y(\omega,t) = \frac{i\mu^2}{\Omega}\sum_{k=1}^{4}(-1)^k e^{iB_k t - \frac{1}{2}\sigma^2 B_k^2}, \tag{16}$$

where

$$A_1 = \omega - 2\Omega + \omega_l, \quad A_2 = \omega + 2\Omega + \omega_l,$$
$$A_3 = \omega + 2\Omega - \omega_l, \quad A_4 = \omega - 2\Omega - \omega_l$$

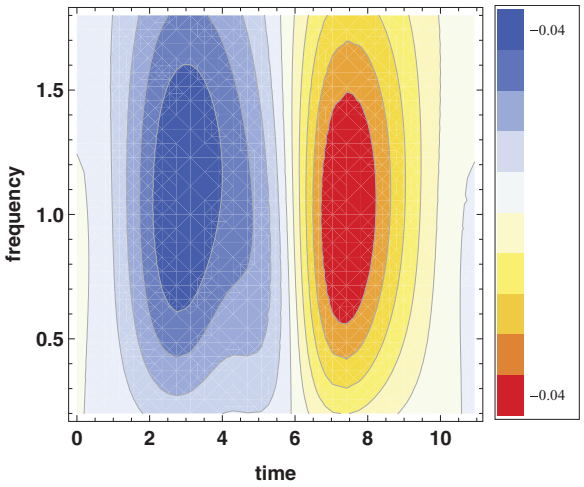

FIG. 9. (Color online) Fourth component $V(\omega,t)$ of the Stokes vector indicating the helicity of the induced polarization in the system ($\omega_l = 1, \sigma = 1, \mu = 0.2, \Delta = 0.05$). The different helicities between absorption (σ_+) and emission (σ_-) phases are evident. Notice the blue-shifting during the absorption phase and the red-shifting of the emission phase. The magnitude of the transition matrix elements μ are exaggerated in order to render the frequency shifting during absorption (blue-shift) and emission (red-shift) phases visible.

and

$$B_1 = \omega - \Omega - \omega_l, \quad B_2 = \omega + \Omega + \omega_l,$$
$$B_3 = \omega - \Omega + \omega_l, \quad B_4 = \omega + \Omega - \omega_l.$$

Note again that the numbering order of A_k and B_k is not the same. From Eqs. (16) it is again possible to derive analytic expressions for the Stokes parameters. Note again that for $\Delta \to 0$ they become the same as in the degenerate case. The common feature of both the degenerate and the quasidegerenate cases is that the terms of the sums have the form $\exp(iA_kt - \frac{1}{2}\sigma^2A_k^2)$ and $\exp(iB_kt - \frac{1}{2}\sigma^2B_k^2)$, so along the time axis we get frequencies A_k (and B_k), while along the ω axis we get Gaussian distributions centered at $\pm 2\Omega \pm \omega_l$ (and $\pm\Omega \pm \omega_l$). Plotting the fourth Stokes parameter reveals an interesting effect of the lift of degeneracy, i.e., the positive helicity during the absorption phase gets slightly blue-shifted, while the negative helicity during the emission phase gets red-shifted. This is of course consistent with the fact that the final state $|b\rangle$ is energetically closer to the intermediate state $|c\rangle$ than that initial state $|a\rangle$ (Fig. 9).

III. FINITE TEMPERATURE

In order to include temperature in a microcanonical ensemble, the most common way is the use of the density matrix, the diagonal elements of which correspond to the population of the several levels due to the temperature distribution (Boltzmann distribution). There is, however, another possibility which turns out to be computationally more practical if one uses wave functions rather than density matrices to propagate the system in time.[33] The idea behind it is that every quantum state which has the correct energy and maximizes the entropy of the system can describe it, thus the thermal distribution is nothing

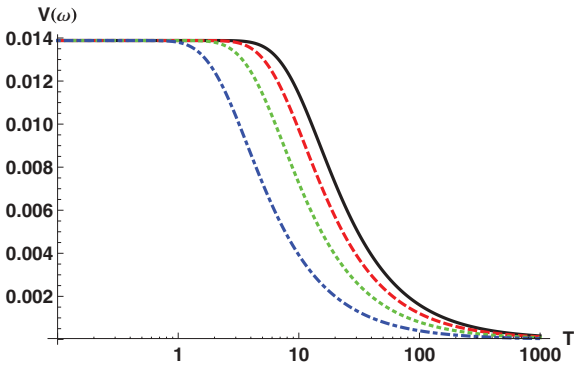

FIG. 10. (Color online) Fourth Stokes parameter as a function of the temperature (logarithmic scale). The values used for the plot are $\omega = \omega_l = E_c = 1$ eV, $\sigma = 1$, $\mu = 0.01$ [note that E_b enters only the population distribution $P_b(0) = b_0$]. The black solid line is for $E_b = 2.0$ meV, the red dashed line for $E_b = 1.5$ meV, the green dotted line for $E_b = 1.0$ meV, and the blue dashed-dotted line for $E_b = 0.5$ meV. Clearly, the signal becomes much weaker but it does not disappear for room temperature.

more than the integral over all such states

$$\psi = \sum_n \lambda_n \psi_n, \tag{17}$$

where ψ_n are the eigenstates of the Hamiltonian. The coefficients λ_n satisfy the convex sum $|\lambda_n|^2 = 1$. Clearly, $|\lambda_n|^2$ is the population P_n of state $|n\rangle$, which practically means that the coefficient λ_n of state $|n\rangle$ in the above expansion is the square root of its population with some arbitrary phase $e^{i\phi_n}$. By using the ergodic theorem, we can calculate the system's response to a laser pulse for the general state and then integrate over all phases. For realistic cases of our Λ system, the intermediate excited state $|c\rangle$ has an energy of the order

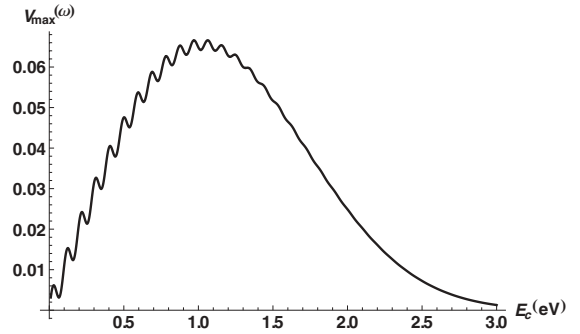

FIG. 11. Fourth Stokes parameter as a function of E_c for $T = 300$ K, $\sigma = 1.0$, $\mu = 0.05$, and $\omega = \omega_l = 1$ eV. The maximum $V(\omega,t)$ value scales with T, but the behavior remains the same (practically only the values of the ordinate axis change). See also Fig. 10. $E_b = 10$ meV. The beatings have frequency $2\sqrt{2}\mu$ and therefore depend on the magnitude of the transition matrix elements, which, at the same time, dictate the speed of the Λ process. μ is set to 0.05 to make the beatings visible.

of 1 eV and thus remains practically unpopulated at room temperature (since $P_c < 5 \times 10^{-6}$ for $T \leqslant 1000$ K, we set approximately $P_c = 0$). Without loss of generality, we can also set the $t = 0$ at a time for which $\phi_a = 0$ (since we will integrate over all phases at the end). So, we change the initial conditions of Eq. (1) to $a(0) = \sqrt{\frac{1}{Z(T)}\exp(-\frac{E_a}{KT})} = \cos\frac{\theta}{2} = a_0$ and $b(0) = e^{i\phi}\sqrt{\frac{1}{Z(T)}\exp(-\frac{E_b}{KT})} = e^{i\phi}\sin\frac{\theta}{2} = e^{i\phi}b_0$, where T is the temperature, K the Boltzmann constant, $Z(T)$ the partition function, and $\phi = \phi_b - \phi_a = \phi_b$ the phase difference between states $|a\rangle$ and $|b\rangle$ at time $t = 0$. The parameters $\{\theta,\phi\}$ give the point on the Bloch sphere for the two states and describe the initial distribution.[34] The solutions now for the general state ψ become

$$a(t) = \frac{1}{2}[a_0 + b_0 e^{i\phi} + a_0\cos(\sqrt{2}\mu t) - b_0 e^{i\phi}\cos(\sqrt{2}\mu t)],$$

$$b(t) = \frac{1}{2}[a_0 + b_0 e^{i\phi} - a_0\cos(\sqrt{2}\mu t) + b_0 e^{i\phi}\cos(\sqrt{2}\mu t)],$$

$$c(t) = -\frac{i}{\sqrt{3}}[(a_0 - b_0 e^{i\phi})\sin(\sqrt{2}\mu t)], \tag{18}$$

which leads to the time-dependent polarization

$$\begin{aligned}\langle D_x(t)\rangle &= \frac{1}{\sqrt{2}}\sin(E_c t)\sin(2\sqrt{2}\mu t)[2a_0 b_0\cos\phi - 1],\\ \langle D_y(t)\rangle &= -\sqrt{2}\sin(\sqrt{2}\mu t)\\ &\quad\times\left[\left(a_0^2 - b_0^2\right)\cos(E_c t) - 2a_0 b_0\sin(E_c t)\sin\phi\right].\end{aligned} \tag{19}$$

Clearly, these still depend on ϕ. Fourier transforming using again a Gaussian distribution as a window function, forming the fourth Stokes parameter $V(\omega,t)$, and integrating over ϕ (random phase approximation[35,36]) leads to

$$\begin{aligned}V(\omega,t) = \tfrac{1}{8}\left(2b_0^2 - 1\right)&e^{-\sigma^2[5\mu^2+3\sqrt{2}\mu(\omega+\omega_l)+(\omega+\omega_l)^2]}\{[-1 + e^{2\sigma^2(3\sqrt{2}\mu+2\omega)\omega_l} - e^{6\sqrt{2}\mu\sigma^2(\omega+\omega_l)} + e^{2\sigma^2\omega(3\sqrt{2}\mu+2\omega_l)}]\cos(\sqrt{2}\mu t)\\ &+ [e^{2\sqrt{2}\mu\sigma^2(\omega+\omega_l)} + e^{4\sqrt{2}\mu\sigma^2(\omega+\omega_l)} - e^{2\sigma^2[2\omega\omega_l+\sqrt{2}\mu(2\omega+\omega_l)]} - e^{2\sigma^2[2\omega\omega_l+\sqrt{2}\mu(\omega+2\omega_l)]}]\cos(3\sqrt{2}\mu t)\\ &- e^{2\sigma^2(2\sqrt{2}\mu+\omega)\omega_l}(e^{6\sqrt{2}\mu\sigma^2\omega} - 1)\cos[(\sqrt{2}\mu - 2\omega_l)t]e^{2\sigma^2[\omega\omega_l+\sqrt{2}\mu(\omega+3\omega_l)]}(e^{2\sqrt{2}\mu\sigma^2\omega} - 1)\cos[(3\sqrt{2}\mu - 2\omega_l t)]\\ &\times e^{2\sigma^2(\sqrt{2}\mu+\omega)\omega_l}(e^{6\sqrt{2}\mu\sigma^2\omega} - 1)\cos[(\sqrt{2}\mu + 2\omega_l)t][e^{2\sigma^2\omega(\sqrt{2}\mu+\omega_l)} - e^{2\sigma^2\omega(2\sqrt{2}\mu+\omega_l)}]\cos[(3\sqrt{2}\mu + 2\omega_l)t]\}.\end{aligned} \tag{20}$$

Equation (20) may seem complicated but it gives insight into the thermal behavior of the helicity signal in a spin-flip experiment. The prefactor $2b_0^2 - 1$ describes the loss of the signal as a function of the initial (thermal) population of the final state $|b\rangle$ (Fig. 10). Another very interesting result is the maximum signal as a function of the energy of the intermediate level E_c (Fig. 11). The signal becomes maximal for $E_c \approx 1$ eV, although the efficiency of every single coherent Λ process is close to 100%. This means that thermal distributions do not completely conceal the effect, which survives in an ensemble measurement. The reason for this is that there is a net contribution to $V(\omega,t)$ from every pure state ψ. The phenomenon is mathematically analogous to the observation that the static phonon contributions to the optical susceptibility of a system as function of the phononic coordinate (and therefore again pertinent to the temperature discussion) do not vanish when integrating over the whole period of the phononic mode, provided that there are some nonlinear contributions (quadratic terms).[37]

IV. CONCLUSIONS

We analytically solve the Λ model system for triplet states under the influence of a spin-flipping laser pulse. We derive a compact analytic form for the time-dependent, induced polarization in the material both in the time and the frequency domain (the latter using a Gaussian window function). We thus show analytically that the process consists of two phases: (i) an absorption phase during which the material absorbs light of σ_+ helicity, and (ii) an emission phase during which the material emits light of σ_- helicity. We find that in a degenerate case, the two helicities occur at the same frequency, while for quasidegenerate cases they are energetically shifted to opposite directions. Our analytical results are in perfect accord with other numerical results and they thus validate each other (to the extent of the approximations done, i.e.. weak perturbations and lifting of degeneracies at least two orders of magnitude smaller than the energetic distance of the intermediate excited states). We also analyze the process starting from a thermal distribution and integrating over all possible relative phases. We find that the averaged induced material polarization becomes weaker but does not completely disappear, thus suggesting that the measured signal in an experiment does not vanish for finite temperatures. Finally, we find that the intensity of the signal depends both on the frequency-measurement time window of the apparatus used (mathematically expressed as σ) as well as on the energy of the intermediate level, although the coherent Λ process can reach as much as 100%. These analytical findings shed new light on the coherent ultrafast spin dynamics. They analytically establish the importance of the light as an angular momentum reservoir during laser-induced spin manipulation in that they consider the irradiated material as an active light source, the polarization of which makes sure that the total angular momentum remains a conserved quantity.

ACKNOWLEDGMENT

We would like to thank the German Research Foundation for financial support through an Individual Grant and the Collaborative Research Center SFB/TRR 88 "3MET."

APPENDIX

The full-windowed Fourier transform of Eq. (14) is

$$\begin{aligned}\tilde{D}_x(\omega,t) = &-\frac{\mu^4 e^{it(\omega+2\Omega-\omega_l)-\frac{1}{2}\sigma^2(\omega+2\Omega-\omega_l)^2}}{\Omega^3} - \frac{\mu^4 e^{it(\omega-2\Omega+\omega_l)-\frac{1}{2}\sigma^2(\omega-2\Omega+\omega_l)^2}}{\Omega^3} + \frac{\mu^4 e^{it(\omega-2\Omega-\omega_l)-\frac{1}{2}\sigma^2(\omega-2\Omega-\omega_l)^2}}{\Omega^3}\\ &+\frac{\mu^4 e^{it(\omega+2\Omega+\omega_l)-\frac{1}{2}\sigma^2(\omega+2\Omega+\omega_l)^2}}{\Omega^3} - \frac{2\mu^2 e^{it(\omega-\omega_l)-\frac{1}{2}\sigma^2(\omega-\omega_l)^2}\Delta}{\Omega^2} + \frac{\mu^2 e^{it(\omega+\Omega-\omega_l)-\frac{1}{2}\sigma^2(\omega+\Omega-\omega_l)^2}\Delta}{\Omega^2}\\ &-\frac{2\mu^2 e^{it(\omega+\omega_l)-\frac{1}{2}\sigma^2(\omega+\omega_l)^2}\Delta}{\Omega^2} + \frac{\mu^2 e^{it(\omega-\Omega+\omega_l)-\frac{1}{2}\sigma^2(\omega-\Omega+\omega_l)^2}\Delta}{\Omega^2} + \frac{\mu^2 e^{it(\omega-\Omega-\omega_l)-\frac{1}{2}\sigma^2(\omega-\Omega-\omega_l)^2}\Delta}{\Omega^2}\\ &+\frac{\mu^2 e^{it(\omega+\Omega+\omega_l)-\frac{1}{2}\sigma^2(\omega+\Omega+\omega_l)^2}\Delta}{\Omega^2} - \frac{\mu^2 e^{it(\omega+\Omega-\omega_l)-\frac{1}{2}\sigma^2(\omega+\Omega-\omega_l)^2}\Delta^2}{\Omega^3} - \frac{\mu^2 e^{it(\omega-\Omega+\omega_l)-\frac{1}{2}\sigma^2(\omega-\Omega+\omega_l)^2}\Delta^2}{\Omega^3}\\ &+\frac{\mu^2 e^{it(\omega-\Omega-\omega_l)-\frac{1}{2}\sigma^2(\omega-\Omega-\omega_l)^2}\Delta^2}{\Omega^3} + \frac{\mu^2 e^{it(\omega+\Omega+\omega_l)-\frac{1}{2}\sigma^2(\omega+\Omega+\omega_l)^2}\Delta^2}{\Omega^3}.\end{aligned}$$

The full-windowed Fourier transform of Eq. (15) is

$$\begin{aligned}\tilde{D}_y(\omega,t) = &\frac{i\mu^2 e^{it(\omega+\Omega-\omega_l)-\frac{1}{2}\sigma^2(\omega+\Omega-\omega_l)^2}}{\Omega} - \frac{i\mu^2 e^{it(\omega-\Omega+\omega_l)-\frac{1}{2}\sigma^2(\omega-\Omega+\omega_l)^2}}{\Omega} - \frac{i\mu^2 e^{it(\omega-\Omega-\omega_l)-\frac{1}{2}\sigma^2(\omega-\Omega-\omega_l)^2}}{\Omega}\\ &+\frac{i\mu^2 e^{it(\omega+\Omega+\omega_l)-\frac{1}{2}\sigma^2(\omega+\Omega+\omega_l)^2}}{\Omega} - \frac{2i\mu^4 e^{it(\omega-\omega_l)-\frac{1}{2}\sigma^2(\omega-\omega_l)^2}\Delta}{\Omega^4} + \frac{2i\mu^4 e^{it(\omega+\Omega-\omega_l)-\frac{1}{2}\sigma^2(\omega+\Omega-\omega_l)^2}\Delta}{\Omega^4}\\ &-\frac{i\mu^4 e^{it(\omega+2\Omega-\omega_l)-\frac{1}{2}\sigma^2(\omega+2\Omega-\omega_l)^2}\Delta}{\Omega^4} + \frac{2i\mu^4 e^{it(\omega+\omega_l)-\frac{1}{2}\sigma^2(\omega+\omega_l)^2}\Delta}{\Omega^4} + \frac{i\mu^4 e^{it(\omega-2\Omega+\omega_l)-\frac{1}{2}\sigma^2(\omega-2\Omega+\omega_l)^2}\Delta}{\Omega^4}\\ &-\frac{2i\mu^4 e^{it(\omega-\Omega+\omega_l)-\frac{1}{2}\sigma^2(\omega-\Omega+\omega_l)^2}\Delta}{\Omega^4} + \frac{2i\mu^4 e^{it(\omega-\Omega-\omega_l)-\frac{1}{2}\sigma^2(\omega-\Omega-\omega_l)^2}\Delta}{\Omega^4} - \frac{2i\mu^4 e^{it(\omega+\Omega+\omega_l)-\frac{1}{2}\sigma^2(\omega+\Omega+\omega_l)^2}\Delta}{\Omega^4}\\ &-\frac{i\mu^4 e^{it(\omega-2\Omega-\omega_l)-\frac{1}{2}\sigma^2(\omega-2\Omega-\omega_l)^2}\Delta}{\Omega^4} + \frac{i\mu^4 e^{it(\omega+2\Omega+\omega_l)-\frac{1}{2}\sigma^2(\omega+2\Omega+\omega_l)^2}\Delta}{\Omega^4} + \frac{2i\mu^2 e^{it(\omega-\omega_l)-\frac{1}{2}\sigma^2(\omega-\omega_l)^2}\Delta^3}{\Omega^4}\\ &-\frac{i\mu^2 e^{it(\omega+\Omega-\omega_l)-\frac{1}{2}\sigma^2(\omega+\Omega-\omega_l)^2}\Delta^3}{\Omega^4} - \frac{2i\mu^2 e^{it(\omega+\omega_l)-\frac{1}{2}\sigma^2(\omega+\omega_l)^2}\Delta^3}{\Omega^4} + \frac{i\mu^2 e^{it(\omega-\Omega+\omega_l)-\frac{1}{2}\sigma^2(\omega-\Omega+\omega_l)^2}\Delta^3}{\Omega^4}\\ &-\frac{i\mu^2 e^{it(\omega-\Omega-\omega_l)-\frac{1}{2}\sigma^2(\omega-\Omega-\omega_l)^2}\Delta^3}{\Omega^4} + \frac{i\mu^2 e^{it(\omega+\Omega+\omega_l)-\frac{1}{2}\sigma^2(\omega+\Omega+\omega_l)^2}\Delta^3}{\Omega^4}.\end{aligned}$$

*lefkidis@physik.uni-kl.de

[1] E. Beaurepaire, J.-C. Merle, A. Daunois, and J.-Y. Bigot, Phys. Rev. Lett. **76**, 4250 (1996).

[2] C. Boeglin, E. Beaurepaire, V. Halté, V. López-Flores, C. Stamm, N. Pontius, H. A. Dürr, and J.-Y. Bigot, Nature (London) **465**, 458 (2010).

[3] U. Atxitia, O. Chubykalo-Fesenko, N. Kazantseva, D. Hinzke, U. Nowak, and R. W. Chantrell, Appl. Phys. Lett. **91**, 232507 (2007).

[4] W. Hübner and G. P. Zhang, Phys. Rev. B **58**, R5920 (1998).

[5] A. M. Kalashnikova, A. V. Kimel, R. V. Pisarev, V. N. Gridnev, A. Kirilyuk, and T. Rasing, Phys. Rev. Lett. **99**, 167205 (2007).

[6] J. Berezovsky, M. H. Mikkelsen, N. G. Stoltz, L. A. Coldren, and D. D. Awschalom, Science **320**, 349 (2008).

[7] J.-Y. Bigot, M. Vomir, and E. Beaurepaire, Nat. Phys. **5**, 515 (2009).

[8] G. Lefkidis, G. P. Zhang, and W. Hübner, Phys. Rev. Lett. **103**, 217401 (2009).

[9] C. Li, W. Jin, H. Xiang, G. Lefkidis, and W. Hübner, Phys. Rev. B **84**, 054415 (2011).

[10] H. P. Xiang, G. Lefkidis, and W. Hübner, Phys. Rev. B **86**, 134402 (2012).

[11] W. Hübner, S. Kersten, and G. Lefkidis, J. Phys.: Conf. Ser. **200**, 042009 (2010).

[12] C. Li, T. Hartenstein, G. Lefkidis, and W. Hübner, Phys. Rev. B **79**, 180413(R) (2009).

[13] G. Lefkidis, M. Blug, H. Kelm, C. Li, G. Pal, H.-J. Krüger, and W. Hübner, J. Phys. Chem. A **115**, 1774 (2011).

[14] W. Jin, F. Rupp, K. Chevalier, M. M. N. Wolf, M. Colindres Rojas, G. Lefkidis, H.-J. Krüger, R. Diller, and W. Hübner, Phys. Rev. Lett. **109**, 267209 (2012).

[15] J. Naudts and W. O. de Calway, Phys. D (Amsterdam) **240**, 542 (2011).

[16] M. Fleischhauer, A. Imamoglu, and J. Marangos, Rev. Mod. Phys. **77**, 633 (2005).

[17] F. T. Hioe and J. H. Eberly, Phys. Rev. Lett. **47**, 838 (1981).

[18] E. Barnes and S. Das Sarma, Phys. Rev. Lett. **109**, 060401 (2012).

[19] B. W. Shore, K. Bergmann, A. Kuhn, S. Schiemann, J. Oreg, and J. H. Eberly, Phys. Rev. A **45**, 5297 (1992).

[20]P. Chen, C. Piermarocchi, L. J. Sham, D. Gammon, and D. G. Steel, Phys. Rev. B **69**, 075320 (2004).
[21]Y. Wu, E. D. Kim, X. Xu, J. Cheng, D. G. Steel, A. S. Bracker, D. Gammon, S. E. Economou, and L. J. Sham, Phys. Rev. Lett. **99**, 097402 (2007).
[22]J. M. Bao, A. V. Bragas, J. K. Furdyna, and R. Merlin, Phys. Rev. B **71**, 045314 (2005).
[23]H. Vonesch and J.-Y. Bigot, Phys. Rev. B **85**, 180407 (2012).
[24]G. P. Zhang, Phys. Rev. B **85**, 224407 (2012).
[25]B. Koopmans, J. J. M. Ruigrok, F. Dalla Longa, and W. J. M. de Jonge, Phys. Rev. Lett. **95**, 267207 (2005).
[26]G. P. Zhang and T. F. George, Phys. Rev. B **78**, 052407 (2008).
[27]Any integral of the form $\int x^i y^j z^k f(r)\,dV$, where $f(r)$ is a spherically symmetric function, vanishes if any of the exponents i, j, or k is an odd integer.
[28]F. T. Hioe, Phys. Rev. A **28**, 879 (1983).
[29]J. R. Kuklinski, U. Gaubatz, F. T. Hioe, and K. Bergmann, Phys. Rev. A **40**, 6741(R) (1989).
[30]Please keep in mind that since RWA keeps the $\omega_0 - \omega_l$ terms but neglects the $\omega_0 + \omega_l$ (where ω_0 is the resonance frequency of the system), the present scheme is not really suitable for treating second harmonic effects.
[31]In order to avoid confusion, we use the terms *helicity* (σ) whenever we refer to the laser pulse and *induced polarization* (**D**) whenever we mean the response of the material. We also use the term *helicity of the induced polarization* for the fourth component of the Stokes vector (V), which describes the circular part of the response of the material.
[32]V. Blanchet, C. Nicole, M.-A. Bouchene, and B. Girard, Phys. Rev. Lett. **78**, 2716 (1997).
[33]J. Naudts and E. Van der Straeten, J. Stat. Mech. : Theor. Exper. (2006) P06015.
[34]F. Bloch, Phys. Rev. **70**, 460 (1946).
[35]D. Pines and D. Bohm, Phys. Rev. **85**, 338 (1952).
[36]It is important to average over ϕ *after* calculating $V(\omega,t)$. In the opposite case, the effect disappears since it is exactly the phase difference between $\langle D_x(t)\rangle$ and $\langle D_y(t)\rangle$ that creates it. Integrating before the windowed Fourier transformation eliminates the phase factors thus erroneously yielding only linear-induced polarization in the material.
[37]G. Lefkidis and W. Hübner, Phys. Rev. B **74**, 155106 (2006).